Article:
Vakurov, A, Drummond-Brydson, R, Ugwumsinachi, O et al. (1 more author) (2016) Significance of particle size and charge capacity in TiO2 nanoparticle-lipid interactions. Journal of Colloid and Interface Science, 473. pp. 75-83. ISSN 0021-9797

https://doi.org/10.1016/j.jcis.2016.03.045

Significance of particle size and charge capacity in TiO_2 nanoparticle-lipid interactions

Alex Vakurov[a], Rik Drummond-Brydson[b], Oji Ugwumsinachi[b] and Andrew Nelson[a]

Schools of [a]Chemistry and [b]Chemical and Process Engineering, University of Leeds, Leeds, LS2 9JT, UK.

Authors' e mail addresses: A.V.Vakourov@leeds.ac.uk, R.M.Drummond-Brydson@leeds.ac.uk, fy12uko@leeds.ac.uk

Corresponding author:

Professor Andrew Nelson

Phone: +44 (0)113 343 6409

Fax: +44 (0)113 343

Email: a.l.nelson@leeds.ac.uk

Abstract

Hypothesis
The activity of submicron sized titanium oxide (TiO_2) particles towards biomembrane models is coupled to their charge carrying capacity and their primary particle size.
Experiments
Electrochemical methods using a phospholipid layer on a mercury (Hg) supported membrane model have been used to determine the phospholipid monolayer activity of TiO_2 as an indicator of biomembrane activity. The particles were characterised for size by dynamic light scattering (DLS) and scanning electron microscopy (SEM) and charge by acid-base titration.
Findings
TiO_2 nanoparticles aggregate in 0.1 mol dm^{-3} solutions of KCl. The charge capacity of TiO_2 nanoparticles depends on their primary particle size and is unaffected by aggregation. TiO_2 particles of < 20 nm primary particle size interact significantly with phospholipid layers. Aggregation of these particles initially has a small effect on this interaction but long term aggregation influences the interaction whereby the aggregates penetrate the lipid layer rather than adsorbing on the surface. Fulvic acid does not inhibit the <20 nm particle/phospholipid interaction. P25 TiO_2 particles of larger particle size interact less strongly with phospholipid layers and the interaction is alleviated following particle aggregation. The semiconductor properties of TiO_2 are evident in voltammograms showing electron transfer to TiO_2 adsorbed on uncoated Hg.

Keywords: Titanium dioxide nanoparticles; Phospholipid monolayers; Rapid cyclic voltammetry; Particle size; Particle aggregation, Semiconductor properties.

Introduction

Titanium dioxide (TiO_2) nanoparticles are one of the most widely used nanomaterials in current application and have extensive use as sunscreens and paints. Accordingly they have a considerable release into environmental systems. Recent estimations have predicted surface water concentrations of discharged TiO_2 to be 21 ng dm^{-3} [1] although these values have yet to be confirmed experimentally. TiO_2 is refractory with a very low water solubility as well as showing a strong tendency to aggregate [2-6]. In spite of this, its biological activity remains uncertain with conflicting reports as to its hazard to environmental and human health [7-10]. A specific feature of TiO_2 is its semiconductor properties which means that the material can absorb UV which enables its photoactivity [11] and photocatalytic activity [12] and may enhance its incipient toxicity [13]. Another property of TiO_2 is its existence in three mineral phases anatase, rutile and brookite respectively [11]. The metastable anatase and brookite phases convert irreversibly to the equilibrium rutile phase upon heating above temperatures in the range 600°-800 °C [14]. Rutile and anatase are the more common forms of TiO_2 with rutile being the most common [11]. In all mineral phases, Ti is octahedrally co-ordinated to oxygen atoms [11].

The aggregation of TiO_2 dispersions in aqueous conditions is mainly due to their lyophobicity promoted by their mineralisation and surface features as well as their overall dimensions [15]. Previous studies in this laboratory have looked at SiO_2 [16,17], ZnO [18] and CdTe [19] nanoparticles correlating their chemical and physical characteristics with their activity towards biological membranes (biomembranes) and/or biomembrane-like layers. Biomembrane activity is defined as the tendency of nanoparticles to structurally modify and /or permeate in, biomembranes and/or biomembrane-like layers. Although SiO_2,ZnO and CdTe nanoparticles differ considerably from each other in their structural properties and functionality, it is shown that for all classes their biomembrane activity is dependent on their particle size. This study continues the theme of relating the physical and chemical properties of nanoparticles to both their electrochemical activity and their activity towards phospholipid model membranes working with representative research grades of TiO_2. The aim of the work is to develop a general model describing the relation between inorganic oxide particle characteristics and their biomembrane activity.

Experimental

Materials

All nanoparticle dispersion concentrations are presented as weight per volume. In the following: TiO_2 nanoparticles employed in this study are described together with their particle sizes in parentheses as quoted by supplier. P25 TiO_2 nanoparticles which are 73 - 85 % anatase, 14 - 17 % rutile and 0 - 18 % amorphous TiO_2 (20-30 nm) [20] was sourced from Degussa. Rutile (30 nm), and a 4:1 mix of anatase and rutile (20 nm) powders respectively and rutile and anatase nanoparticle (5-15 nm) dispersions in water (15% w/v, 99.9% purity) were obtained from US Research Nanomaterials, Inc. The anatase and rutile dispersions are referred to as “stock dispersions” in the remainder of the paper. 1,2-dioleoyl-sn-glycero-3-phosphocholine (DOPC) was purchased from Avanti Polar Lipids and had a purity of >99%. Analytical grade NaOH, KNO_3 and 70% HNO_3 were purchased from Sigma-Aldrich. All glassware was rinsed before use with MilliQ 18.2MΩ water (Millipore, U.K). Piranha solution used to treat the Pt electrodes consists of H_2SO_4 (Fisher Scientific) and H_2O_2 (Sigma-Aldrich) in a 3:1 ratio respectively.

Dynamic light scattering (DLS) and scanning electron microscopy (SEM)

The stability of TiO_2 nanoparticles in various media was measured using DLS on a nanoZS zetasizer (Malvern Instruments Ltd.). The media tested consisted of MilliQ water and 0.1 mol dm^{-3} KCl. Samples for DLS assay were prepared by adding 10 µL of 10% w/v TiO_2 dispersions into a cuvette containing 1 cm^3 of the desired media to give a testing concentration of 0.1% TiO_2. All dispersions were sonicated for 1 minute prior to DLS analysis. In the SEM measurements, a 0.1 cm^3 sample was deposited on to a SEM stub and dried within a stream of nitrogen gas (Air Products). The nanoparticle samples were sputter coated with a 3 nm thick Pt/Pd layer prior to SEM imaging. SEM imaging was carried out at 3 kV on a LEO 1530 Gemini FEG-SEM (Carl Zeiss ZMT) with an Oxford Instruments AZtecEnergy EDX system attached. Anatase and rutile "stock

dispersions" were also tested but were not mixed with any media as they were already fully dispersed.

Charge-pH measurements

10% dispersions of each TiO_2 sample were prepared by the addition of 20 g of nanoparticles to 200 cm^3 of MilliQ water (Millipore, U.K) in plastic beakers. The dispersion was then brought to pH 2 by the dropwise addition of 75% HNO_3 and sonicated in a Branson 2100 sonicator for 2 hours. Samples were stored in plastic bottles at 25^{O}C for a maximum of 1 week before being purified by dialysis. Purification of nanoparticle dispersions is necessary since any impurities and salts that may be present as a result of the manufacturing process must be removed in order to determine surface charge accurately. Dialysis was carried out in MilliQ water using dialysis tubing (Visking 1350/2) that had been heated to 100^{O}C in MilliQ water for two minutes and allowed to cool. All Visking tubes were rinsed successively with MilliQ water to remove any major impurities. TiO_2 dispersions were ultrasonicated for one hour prior to dialysis to ensure maximum disaggregation. Dialysis was carried out against MilliQ water for three days. Following dialysis the dispersions were re-adjusted to pH 2 by addition of HNO_3. They were then ultrasonicated for one hour to ensure stability. All samples were used within 1 month of purification. 25 cm^3 of 10% w/v nanoparticle dispersion was diluted with 25 cm^3 of 0.2, 0.02 and 0 mol dm^{-3} KNO_3 to give 5% TiO_2 in 0.1, 0.01 and 0 mol dm^{-3} KNO_3 respectively in a 100 cm^3 beaker. The TiO_2 dispersions were titrated with 0.1 mol dm^{-3} NaOH to pH 9-10 under conditions of constant stirring. The solution pH was measured using a Corning pH Meter 240. In the analysis, the H^+ ions titrated as estimated from the pH value were subtracted from the moles of NaOH added to give the titrated H^+ ions adsorbed on the TiO_2. The error in this estimation due to the depression of the H^+ activity by the ionic strength is within the error of the pH measurement [21]. An additional complication is the fact that the H^+ activity can be increased in the presence of colloidal dispersions [22] contributing an error if the pH of the dispersion is compared to that of a pure solution. An advantage therefore of estimating the H^+ titrated from the pH value of the TiO_2 dispersion is that it represents an internal control. Relative charge per gram TiO_2 was plotted against the solution pH. The absolute charge values were obtained by subtracting the charge value found at the solution pH equivalent to the position of zero charge (PZC) of TiO_2, from the relative charge value. The PZC of TiO_2 is the point where zero charge resides on the particle surface. The pH value of the TiO_2 dispersion equivalent to the PZC of TiO_2 was determined by measuring the pH of a concentrated (~15%) *pure* dispersion [23]. To do this a TiO_2 dispersion acidified to pH 2 was ultrasonicated and dialysed as above. It was then brought to pH 7 by addition of 0.1 mol dm^{-3} NaOH. Following this, it was dialysed until the dispersion pH reached a constant value. For all dispersions, this was recorded as pH 6.3 +/- 0.15. This value was generally in agreement with the literature value for the pH value in equilibrium with the PZC of TiO_2 [23] and was used throughout to obtain absolute charge values for the TiO_2 samples.

Electrochemical measurements

The electrochemical testing system used consisted of a peristaltic pump (Cole-Parmer Instrument Co.), a 10 dm^{-3} electrolyte reservoir, a 25 cm^3 sample cell and a 0.75 cm^3 flow cell constructed of Plexiglas [16,18]. Two universal valve switch modules (Anachem Ltd.) were used to control the supply of either electrolyte or test sample to the pump and all mechanical components were connected with rubber tubing. The contents of both the electrolyte reservoir and sample cell were constantly stirred by magnetic stirrers and aerated with argon (Air Products) prior to each test. The working electrode consisted of a microfabricated one mm Pt electrode base (Tyndall National Institute, Ireland) on a silicon wafer with an electrodeposited Hg surface as Hg film electrode (MFE) [24]. The auxillary electrode was a rectangular Pt film fabricated on the wafer. The Pt electrodes were first cleaned with piranha solution and rinsed with MilliQ water. They were then dried with a stream of N_2 and the wafer was placed in the flow cell. 50 *m*mol dm^{-3} $Hg(NO_3)_2$ solution was passed through the flow cell at a rate of 5 cm^3 min^{-1}. Reduction of Hg on to the Pt electrode occurred at -0.4V vs Ag/AgCl. Subsequent to electrodeposition, the electrode was washed with a stream of MilliQ water. A Ag/AgCl 3 mol dm^{-3} KCl REF 201 electrode (VWR International Ltd.) was placed in the flow cell as reference and all potentials in this paper are quoted against this. All electrodes were connected to a PGSTAT 30 Autolab potentiostat (Ecochemie, Utrecht, The Netherlands). Rapid cyclic voltammetry (RCV) was carried out in 0.1

mol dm^{-3} KCl + 0.01 mol dm^{-3} phosphate (PBS) electrolyte at pH 7.4 with a total ionic strength of 0.125 mol dm^{-3}. Additional experiments in 0.1 mol dm^{-3} KCl showed that the phosphate had no effect on the TiO_2 interaction with the DOPC layers. 300 µL of DOPC dispersion of concentration 0.254 μm cm^{-3} was injected into the flow cell at a rate of 1 cm^3 min^{-1} applying RCV from -0.4V to -3V at 80 Vs^{-1}. Following the appearance of the DOPC voltammetric peaks, RCV was restarted at a voltage excursion of -0.4 to -1.625V to test the integrity of the DOPC monolayer. Subsequently the potential was switched off and electrolyte was replaced with a 0.1% dispersion of TiO_2 in MilliQ water in the flow cell. The electrode was exposed for 30 seconds to the TiO_2 dispersion. In one experiment the electrode was exposed to 0.1% TiO_2 dispersion in soil water containing 5 mg dm^{-3} humic acid. The TiO_2 dispersion was replaced with electrolyte, the electrode was tested by RCV from -0.4V to -1.125V and in some cases to -1.8 V at 40Vs^{-1} and scans were taken at 1 second intervals for 30 seconds. RCV was then terminated and the system washed through with electrolyte at a flow rate of 10 cm^3 min^{-1}. RCV was restarted from -0.4V to -3V at 80Vs^{-1} to clean the Hg electrode, at which point all voltammetric peaks disappeared indicating monolayer removal and only the uncoated Hg and electrolyte remained. Following this, the DOPC layer was re-deposited as described above. This monitoring/cleaning/redeposition process was repeated as described above for as long as it was necessary to take measurements. Measurements on an uncoated Hg electrode were carried out in the same way with the same TiO_2 dispersions in MilliQ water. In this case the Hg was cleaned in between measurements using the same procedure as described above for removing the DOPC layer.

Results and discussion

Figure 1 summarises the DLS results for all the samples. It is noted that the particle sizes as determined by DLS bear little relation to those quoted by the supplier. SEM results for the particles displayed in Figure 2 also show little agreement as seen by eye with the supplier's values and show varying degrees of aggregation in particular the rutile (Figure 2(b)) and anatase/rutile (Figure 2(c)) powders. The DLS results indicate that in the presence of 0.1 mol dm^{-3} KCl, TiO_2 particles aggregate and the extent of aggregation is variable. Interestingly the anatase "stock dispersion" showed the smallest primary particle size at 16 nm confirmed by SEM in Figure 2(e) which suggests a relatively monodispersed sample. This sample was the most stable aggregating to 67 nm after 30 minutes incubation in 0.1 mol dm^{-3} KCl. There is some correlation between the samples in Figures 1 and 2 in particular the primary peak in DLS and the SEM images but the drying effects in SEM samples will have an effect. The secondary peak in DLS is not observed at this SEM magnification. The charge-pH plots are displayed in Figure 3. Their derivation from the titration is summarised in the inset to Figure 3(a) which displays plots of moles NaOH added versus moles H^+ titrated calculated from *in-situ* pH measurements. It is evident that at low pH values the plots overlay each other since the TiO_2 is saturated with protons and only the solution H^+ is titrated whereas at higher pH values the H^+ dissociated from the particle surface is titrated. The overlay of the results at the low dispersion pH value confirms the validity of the experimental analysis taken. The main plot in Figure 3(a) indicates that the P25 dispersion has a charge capacity of more than twice as much as the rutile "stock disperson" and the rutile and anatase/rutile powder dispersions. This charge-capacity relates to its particle size as shown by DLS which is smaller than that of the other particle samples except for the anatase "stock dispersion". Figure 3(b) shows that the anatase "stock dispersion" holds the highest charge on its surface relating to its smallest particle size as indicated by DLS. Interestingly for all particle dispersions, the charge carried increases with increasing ionic strength (Figure 3(c)) as shown previously due to increased counter-ion association [23].

Figure 4 shows the effect of the particle dispersions on the voltammograms of uncoated Hg. In this case an increase in current is seen in relation to an increase in negative potential commencing at ~ -0.8 V. This increase in current is significant when the uncoated electrode is exposed to P25 (Figure 4(a)) and is highest when exposed to the anatase "stock dispersion" (Figure 4(e)). The ranking of current increase is related to the particles' charge carrying capacity. The semiconductor effect is similar to that observed when uncoated Hg electrodes were exposed to ZnO particle dispersions [18]. The increase in current can therefore be related to the semiconductor properties of TiO_2 and the injection of electrons under applied potential into the conduction band of

TiO_2. This effect has been observed previously on nanocrystalline TiO_2 electrodes in aqueous electrolyte [25]. The TiO_2 is adsorbed on the electrode since following incubation with the TiO_2 dispersion in MilliQ water, the electrode was monitored by RCV with pure electrolyte in the flow cell. Figure 5 displays the voltammograms of the DOPC coated electrode exposed to the TiO_2 dispersions. As noted previously [16], adsorption of particles on the DOPC surface is seen as a depression of the capacitance current peaks on the voltammogram. The P25 dispersion interacts to a small extent with the lipid layer (Figure 5(a)) correlating with its increased charge capacity while three of the other TiO_2 dispersions show insignificant interaction with the DOPC layer (Figures 5(b), 5(c) and 5(d). The anatase "stock dispersion" interacts strongly with the DOPC layer as evidenced by the almost complete suppression of the capacitance current peaks after 30 *s* exposure to a 0.1% TiO_2 dispersion in MilliQ water (Figure 5(e)). The P25 interaction was probed more extensively by recording voltammograms with a greater voltage excursion to -1.8 V. This is displayed in Figure 6(a) where the interaction of the P25 dispersion in MilliQ water with the DOPC is clearer, exemplified by the increase in current at potentials more negative than those characterising the DOPC reorientations. This is caused by electron transfer to TiO_2 brought close to the electrode surface following the DOPC structural transitions. Interestingly following incubation of the dispersion in 0.1 mol dm^{-3} KCl for one minute, the interaction is greatly decreased (Figure 6(b)) and is similar to that of the remaining TiO_2 dispersions in MilliQ water as exemplified by the effect of the rutile powder dispersion on DOPC layers (Figure 6(c)). This indicates that P25 nanoparticle aggregation in 0.1 mol dm^{-3} KCl decreases its activity towards the DOPC layer.

Figure 7 shows the effect of the incubation of the anatase “stock dispersion” for 30 minutes in 0.1 mol dm^{-3} KCl where there is some particle aggregation to 67 nm (Figure 1(e)). A strong interaction of the dispersion with the DOPC layer remains as shown in Figure 7(a). Interestingly after 8 hours incubation with 0.1 mol dm^{-3} KCl, the interaction of an aggregated anatase "stock suspension" with the DOPC layer is altered whereby the depression of the capacitance peak current is lessened but an increase in the baseline capacitance current with increasing negative potential is observed (Figure 7(b). This baseline increase can be better interpreted following sight of the same in the RCVs in Figure 4 which arises from electron transfer to electrode-adsorbed TiO_2 particles. Accordingly the baseline increase in Figure 7(b) corresponds to electron transfer to TiO_2 aggregates which have penetrated through the lipid layer to the Hg surface. The aggregates have lower affinity for the monolayer surface due to their increased particle size which allows their penetration into the layer to take place. Of interest also is that TiO_2 particle dispersions in fulvic acid media display strong interaction with the DOPC layer (Figure 7(c)) which is in contrast to ZnO particle dispersions where the fulvic acid alleviates interactions between the particles and the lipid. Stabilisation of the small TiO_2 particle size by fulvic acid has been reported [26] and this would enhance interaction with DOPC as observed by the effect of dispersant on ZnO interaction [18]. On the other hand, it is considered that the solubility of ZnO to Zn^{2+} ion will facilitate complexation of Zn(II) fulvate complex [27] on the surface of ZnO which may inhibit the interaction of ZnO with the lipid. Figure 7(d) confirms that the fulvic acid itself does not interact with the DOPC layer [18].

Conclusions

A summary of the findings.

TiO_2 nanoparticles show a strong tendency to aggregate in media of ionic strength ~ 0.1 mol dm^{-3} KCl. Their charge holding capacity depends on their primary particle size and is unaffected by their aggregation. TiO_2 particles below primary particle size 20 nm interact strongly wth DOPC layers. Aggregation of these particles has a small effect on this interaction but long term aggregation influences the interaction whereby the aggregates penetrate the lipid layer rather than adsorbing on the surface. The significant interaction of the P25 dispersion with the DOPC layer as compared to the remaining dispersions is related to its charge holding capacity which is higher and its primary particle size which is smaller than the other dispersions excepting the anatase "stock dispersion". The semiconductor properties of TiO_2 are shown in the voltammograms of uncoated Hg and can be used as a probe to indicate penetration of the DOPC layers by the TiO_2 in particular at higher applied potentials than those characterising the DOPC reorientations. The semiconductor properties are also related to the particles' charge carrying capacity and inversely related to their particle size.

A synopsis of your new concepts and innovations.

A proven concept in this study is the coupling of TiO_2 particle biomembrane activity, charge carrying capacity and primary size. An additional significant concept is that aggregates of the smallest size TiO_2 particles can retain their phospholipid layer activity and their charge carrying capacity since they are necessarily loosely bound at least initially.

A brief restatement of your hypotheses.

The biomembrane activity of TiO_2 particles is coupled with their charge carrying capacity and primary particle size.

A comparison with findings by other workers [give references].

The aggregation of TiO_2 nanoparticles follows that of ZnO nanoparticle aggregation [18]. The biomembrane activity of TiO_2 nanoparticles with primary particle size below 20 nm can be compared to that of SiO_2, ZnO and CdSe and CdTe nanoparticles [16-19]. A significant difference between TiO_2/DOPC and ZnO/DOPC interaction is that solution fulvic acid and phosphate does not inhibit the <20 nm particle interaction which is probably associated with the insolubility of TiO_2 compared with the ability of ZnO to release Zn^{2+} ion to aqueous solution [18]. The semiconductor properties of TiO_2 observed in their voltammetry is similar to that of ZnO nanoparticles and has been observed by other workers using similar electrochemical methods [25].

Your vision for future work.

Future work in this area should compare the effects of TiO_2 nanoparticles on the electrochemical membrane model with other membrane models in particular vesicles to exactly elucidate the interaction mechanism using direct imaging methods such as confocal microscopy.

Acknowledgements.

This work was part of the ENNSATOX programme funded by EU FP7 under grant agreement no. NMP-229244. Many thanks to project student Harris Jammaluddin for carrying out the initial TiO_2 titrations. Characterised soil water was provided by Dr Claus Svendsen from the NERC Centre for Ecology and Hydrology, Wallingford, UK.

References.

[1] Gottschalk F, Sonderer T, Scholz R W and Nowack B 2009 Modeled environmental concentrations of engineered nanomaterials (TiO_2, ZnO, Ag, CNT, Fullerenes) for different regions *Environ. Sci. Technol.* 43 9216–9222

[2]. Romanello M B and Fidalgo de Cortalezzi M M 2013 An experimental study on the aggregation of TiO_2 nanoparticles under environmentally relevant conditions. *Water Res.* 47 3887-98

[3] Chowdhury I Walker S L and Mylon S E 2013 Aggregate morphology of nano-TiO2: role of primary particle size, solution chemistry, and organic matter *Environ. Sci.: Processes Impacts* 15 275–282

[4] Sillanpää M Paunu T-M and Sainio P 2011 Aggregation and deposition of engineered TiO_2 nanoparticles in natural fresh and brackish waters *Journal of Physics:Conference Series* 304 012018 1-8

[5] Keller A A Wang H Zhou D Lenihan H S Cheer G Cardinale B J Miller R and Zhaoxia J I Stability and aggregation of metal oxide nanoparticles in natural aqueous matrices 2010 *Environ. Sci. Technol.* 44, 1962–1967

[6] Guzman K A D Finnegan M P and J.F. Banfield J F 2006 Influence of surface potential on aggregation and transport of titania nanoparticles *Environ. Sci. Technol.* 40 7688-7693.

[7] Kim E Kim S-H Kim H-C Lee S G Lee S J and. Jeong S W 2011 Growth inhibition of aquatic plant caused by silver and titanium oxide nanoparticles. *Toxicology and Environmental Health Science* 3 1-6

[8] Dabrunz A Duester L Prasse C Seitz F Rosenfeldt R Schilde C Schaumann G E Schulz R 2011 Biological surface coating and molting inhibition as mechanisms of TiO_2 nanoparticle toxicity in *Daphnia magna* *Plusone* 6 e20112 1-7

[9] Lai J C K Lai M B Jandhyam S Dukhande V V Bhushan A Daniels C K and Leung S W 2008 Exposure to titanium dioxide and other metallic oxide nanoparticles induces cytotoxicity on human neural cells and fibroblasts *International Journal of Nanomedicine* 3 533-545

[10] Hartmann N B Von der Kammer F Hofmann T Baalousha M Ottofuelling S and Baun A 2010 Algal testing of titanium dioxide nanoparticles-Testing considerations, inhibitory effects and modification of cadmium bioavailability *Toxicology* 269 190-197
[11] Landmann M Rauls E and Schmidt W G 2012 The electronic structure and optical response of rutile, anatase and brookite TiO_2 *J. Phys.: Condens. Matt*er 24 195503 1-6
[12] Tian G Fu H Jing L Xin B and Pan K Preparation and characterization of stable biphase TiO2 photocatalyst with high crystallinity, large surface area, and enhanced photoactivity 2008 *J. Phys. Chem. C* 112 3083-3089
[13] Hongbo M A Brennan A and Diamond S A 2012 Phototoxicity of TiO_2 nanoparticles under solar radiation to two aquatic species: *Daphnia magna* and Japanese medaka *Environmental Toxicology and Chemistry* 31 1621–1629
[14] Greenwood N N and Earnshaw A 1984 Chemistry of the Elements. Oxford: Pergamon Press. pp. 1117–19. ISBN 0-08-022057-6.
[15] Kallay N and Zalac S 2002 Stability of nanodispersions: A model for kinetics of aggregation of nanoparticles *Journal of Colloid and Interface Science* 253 70-76
[16] Vakurov A Brydson R Nelson A 2012 Electrochemical modeling of the silica nanoparticle-biomembrane interaction *Langmuir* 28 1246-1255.
[17] Zhang S Nelson A Beales P A 2012 Freezing or wrapping: the role of particle size in the mechanism of nanoparticle−biomembrane interaction *Langmuir* 28:12831-12837.
[18] Vakurov A Mockry G Nelson A Drummond-Brydson R Wallace R Svendsen C 2013 ZnO nanoparticle interactions with phospholipid monolayers *Journal of Colloid and Interface Science*, 404 161–168
[19] Zhang S Chen R Malhotra G Vakurov A Nelson A Critchley K 2014 Electrochemical modelling of QD-phospholipid interactions *Journal of Colloid and Interface Science* 420 9-14
[20] Ohtani B Prieto-Mahaney O O Li D Abe R 2010 What is Degussa (Evonik) P25? Crystalline composition analysis, reconstruction from isolated pure particles and photocatalytic activity test *Journal of Photochemistry and Photobiology A-Chemistry* 216 179-182
[21] Harris DC 2003 Quantitative Chemical Analysis. New York: WH Freeman and Company. p. 156. ISBN-13: 978-0716744641.
[22] Sparks DL 1984 Ion activities: An historical and theoretical overview *Soil Science Society of America Journal* 48 514-518
[23] Preocanin T and Kallay N 2006 Point of zero charge and surface charge density of TiO_2 in aqueous electrolyte solution as obtained by potentiometric mass titration *Croatica Chemica Acta* 79 95-106
[24] Coldrick Z Penezic A Gasparovic B Steenson P Merrifield J Nelson A 2011 High throughput systems for screening biomembrane interactions on fabricated mercury film electrodes *J Appl Electrochem* 41 939-949
[25] Fabregat-Santiago F Mora-Sero I Garcia-Belmonte G and Bisquert J 2003 Cyclic voltammetry studies of nanoporous semiconductors. capacitive and reactive properties of nanocrystalline TiO_2 electrodes in aqueous electrolyte J Phys Chem B 107 758-768
[26] Domingos R F Tufenkji N Wilkinson K J 2009 Aggregation of titanium dioxide nanoparticles: role of a fulvic acid *Environmental Science and Technology* 43 1283-1286
[27] Cheng, E T De Schamphelaere K Lofts, S Janssen C Allen H E Measurement and computation of zinc binding to natural dissolved organic matter in European surface waters 2005 *Analytica Chimica Acta* 542 230-239

Figure legends

Figure 1

DLS number particle size distribution of 0.1% dispersions of: (a) P25, (b) rutile powder, (c) mixed anatase/rutile (4:1) powder, (d) rutile "stock dispersion" and, (e) anatase "stock dispersion" in, MilliQ water (black line), 0.125 mol dm^{-3} PBS (red line) and (e) in 0.125 mol dm^{-3} PBS, incubation time: 1 (red dash line), 15 (purple line) and 30 min (blue line).

Figure 2

SEM images of dried 0.1% dispersions of (a) P25, (b) rutile powder, (c) mixed anatase/rutile (4:1) powder, (d) rutile "stock dispersion" and, (e) anatase "stock dispersion".

Figure 3

Charge per mass (coulomb g^{-1}) versus solution pH of 5% (a) P25 (solid triangle), rutile powder (solid circle), mixed anatase/rutile (4:1) powder (open square) and rutile "stock dispersion" (cross), in 0.1 mol dm^{-3} KCl, (b) anatase (open triangle) and rutile (cross) "stock dispersions" and, (c) P25 in 0.1 (solid triangle), 0.01 (open circle) and 0 (diagonal cross) mol dm^{-3} KCl. Inset to (a) moles of added NaOH (solid triangle) and moles titrated solution H^+ (open circle) calculated from *in-situ* pH, versus pH of 5% rutile “stock dispersion”.

Figure 4

RCV (scan rate 40 Vs^{-1}) of uncoated MFE in 0.125 mol dm^{-3} PBS at pH 7.4 before (black line) and after (red line) exposure to 0.1% (a) P25, (b) rutile powder, (c) mixed anatase/rutile (4:1) powder, (d) rutile "stock dispersion" and, (e) anatase "stock dispersion" in MilliQ water.

Figure 5

RCV (scan rate 40 Vs^{-1}) of DOPC coated MFE in 0.125 mol dm^{-3} PBS at pH 7.4 before (black line) and after (red line) exposure to 0.1% (a) P25, (b) rutile powder, (c) mixed anatase/rutile (4:1) powder, (d) rutile "stock dispersion" and, (e) anatase "stock dispersion" in MilliQ water.

Figure 6

RCV (scan rate 40 Vs^{-1}) of DOPC coated MFE in 0.125 mol dm^{-3} PBS at pH 7.4 before (black line) and after (red line) exposure to (a) 0.1% P25 in MilliQ water, (b) 0.1% P25 incubated for one minute in 0.125 mol dm^{-3} PBS at pH 7.4 (c) rutile powder in MilliQ water.

Figure 7

RCV (scan rate 40 Vs^{-1}) of DOPC coated MFE in 0.1 mol dm^{-3} PBS before (black line) and after (red line) exposure to 0.1% anatase "stock dispersion", incubated for (a) 30 minutes and (b) 480 minutes, in 0.1 mol dm^{-3} KCl and (c) in 10% soil water containing 5 mg dm^{-3} fulvic acid, and DOPC coated MFE exposure to (d) 10% soil water containing 5 mg dm^{-3} fulvic acid.

5: Figure

Figure 1

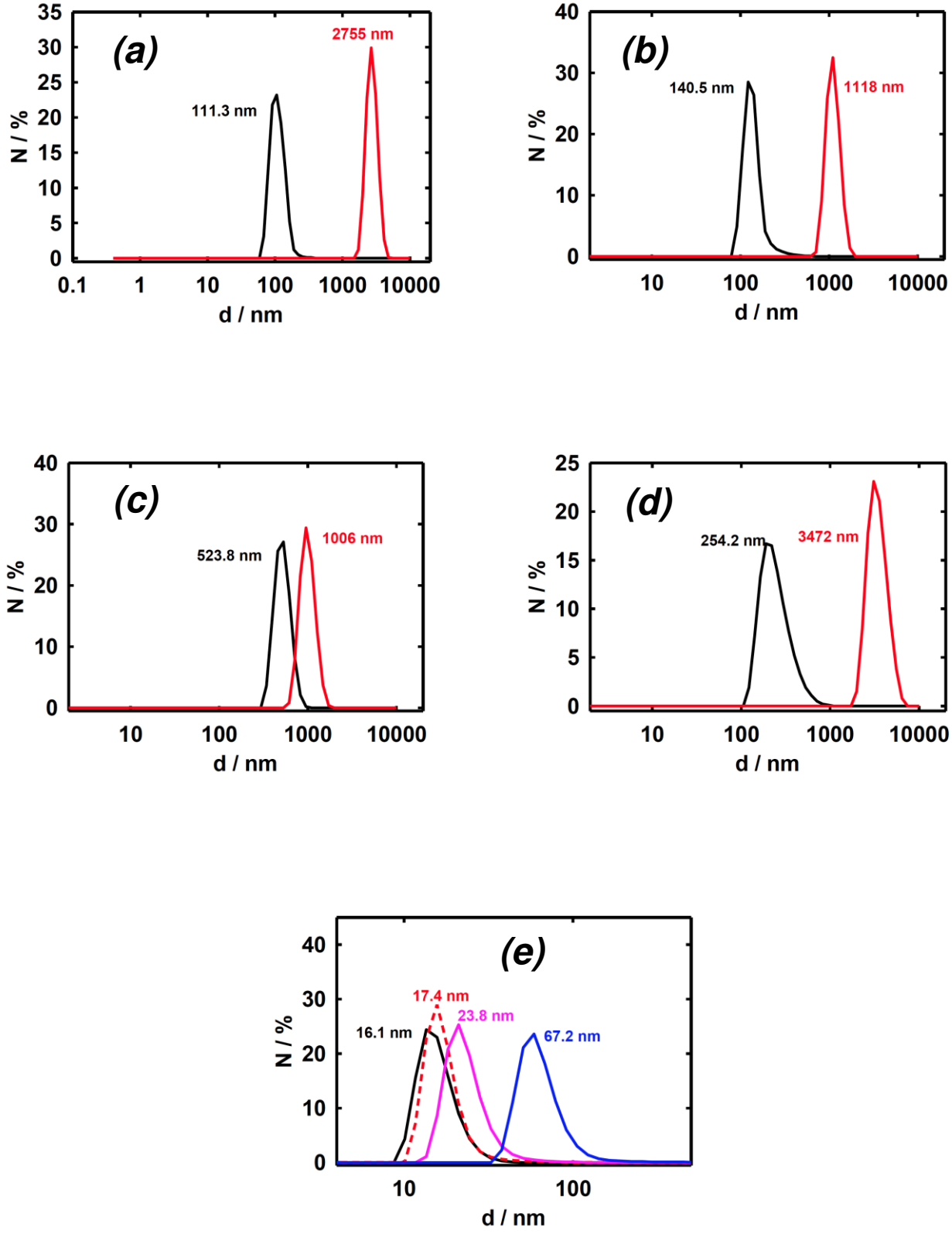

5: Figure

Figure 2

(a)

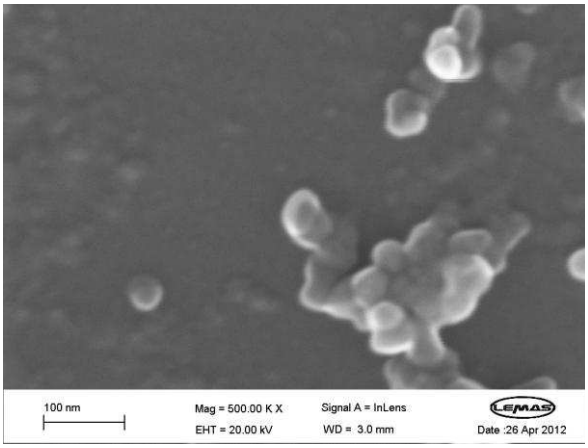

(b)

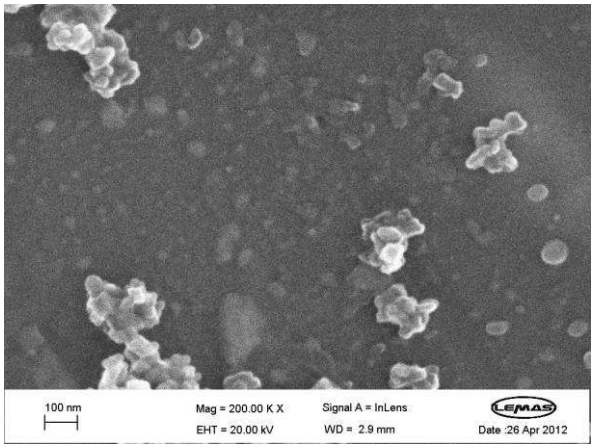

(c)

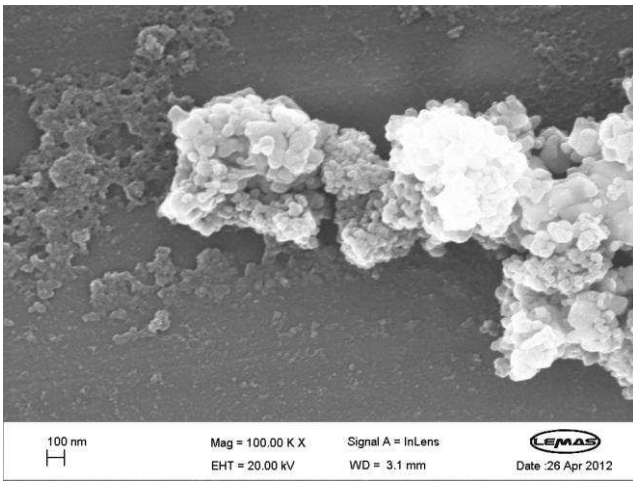

(d)

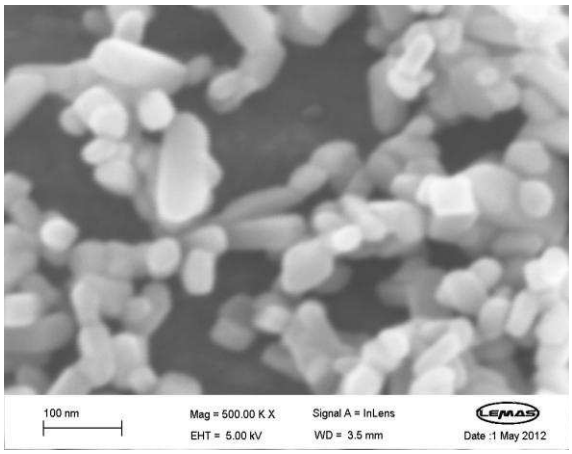

(e)

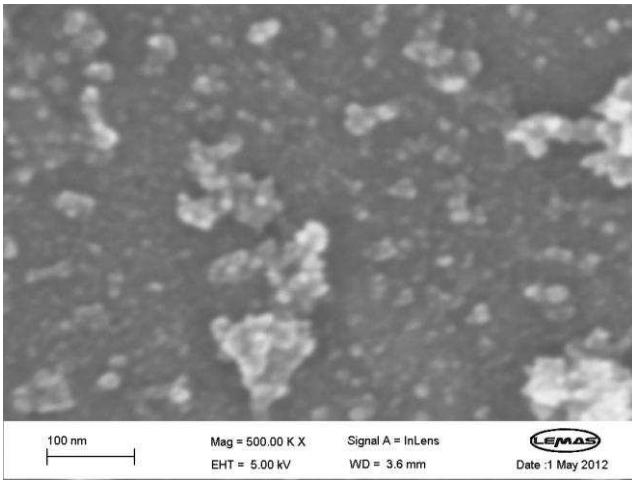

5: Figure

Figure 3

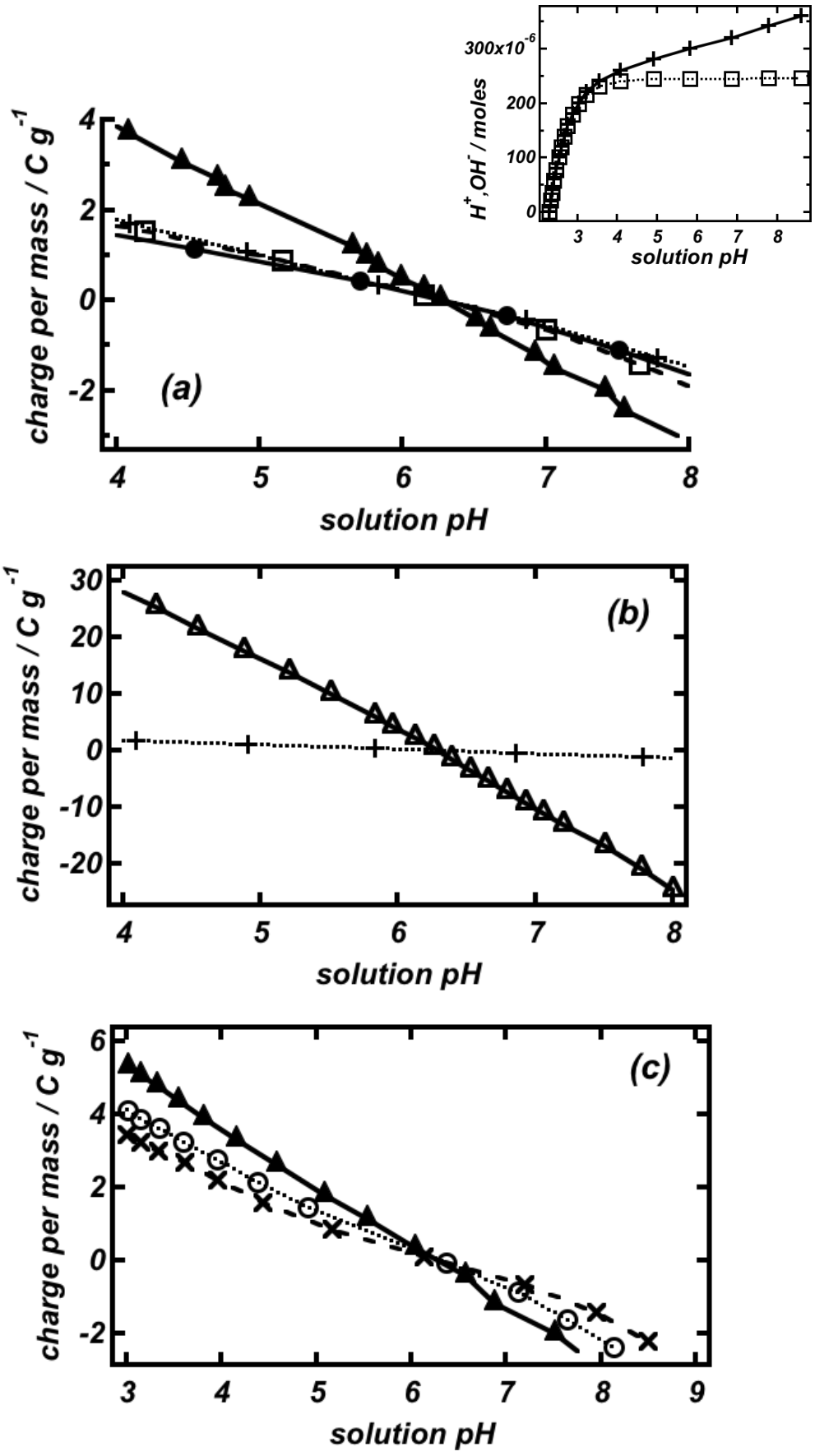

5: Figure

Figure 4

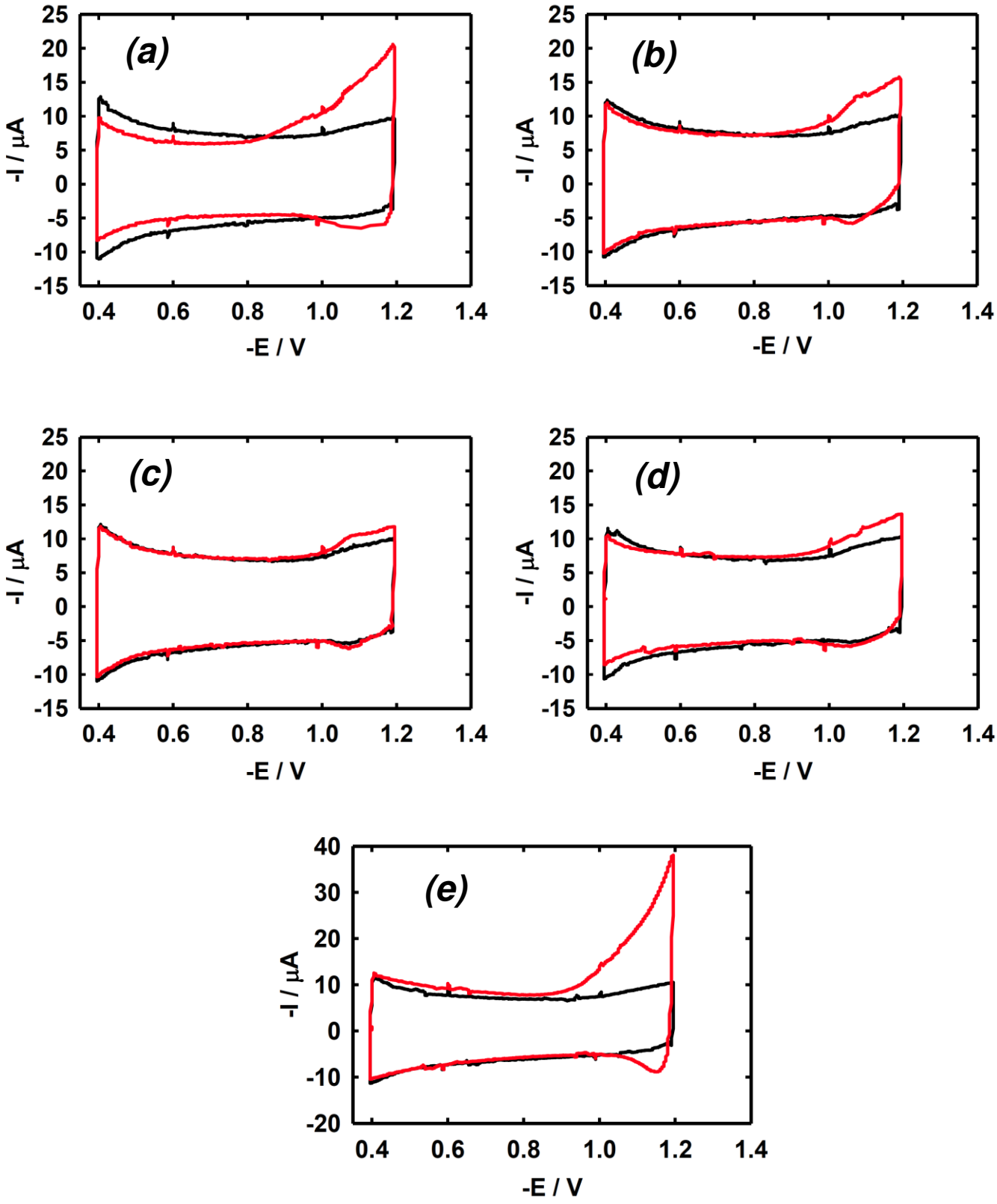

Figure 5

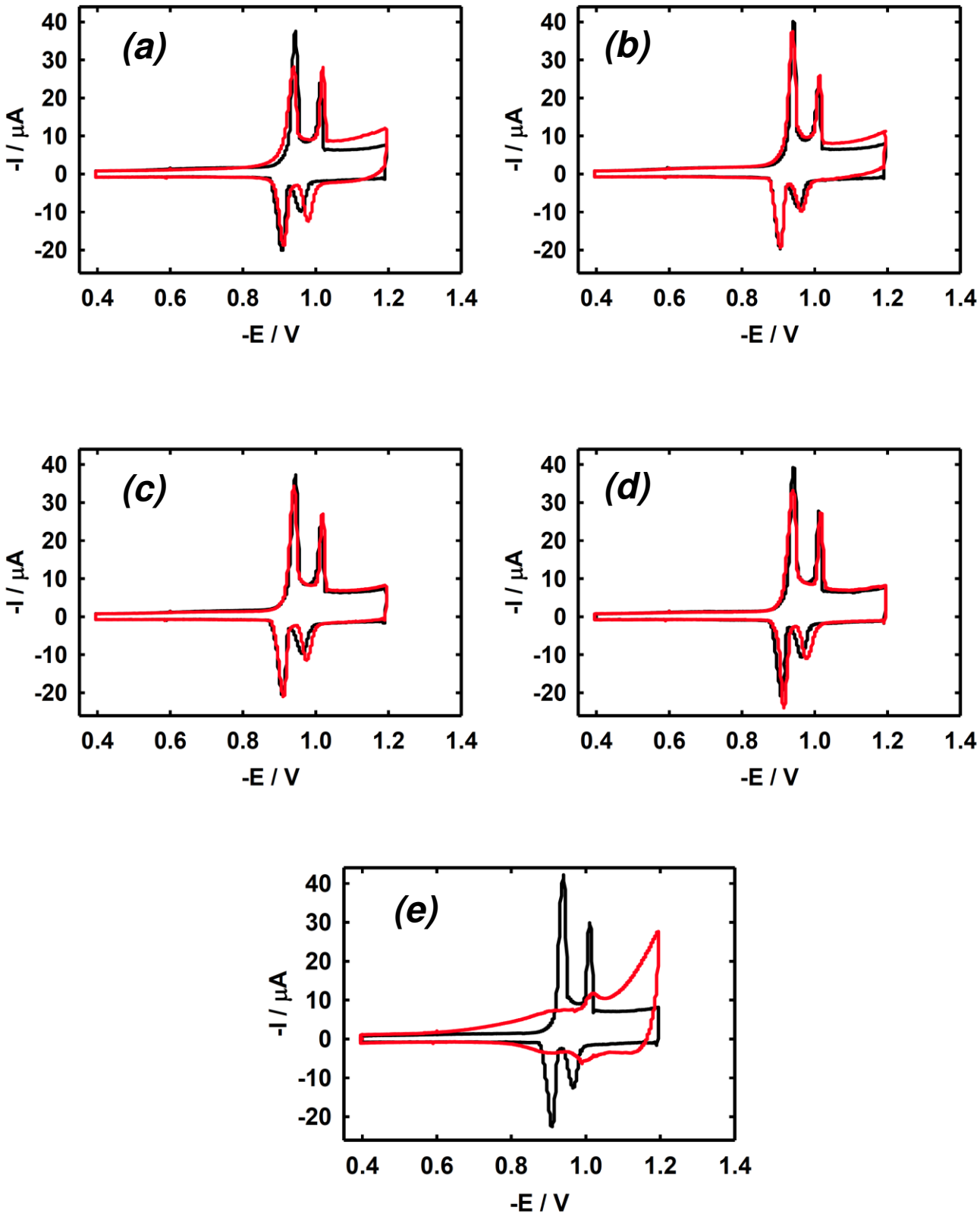

Figure 6

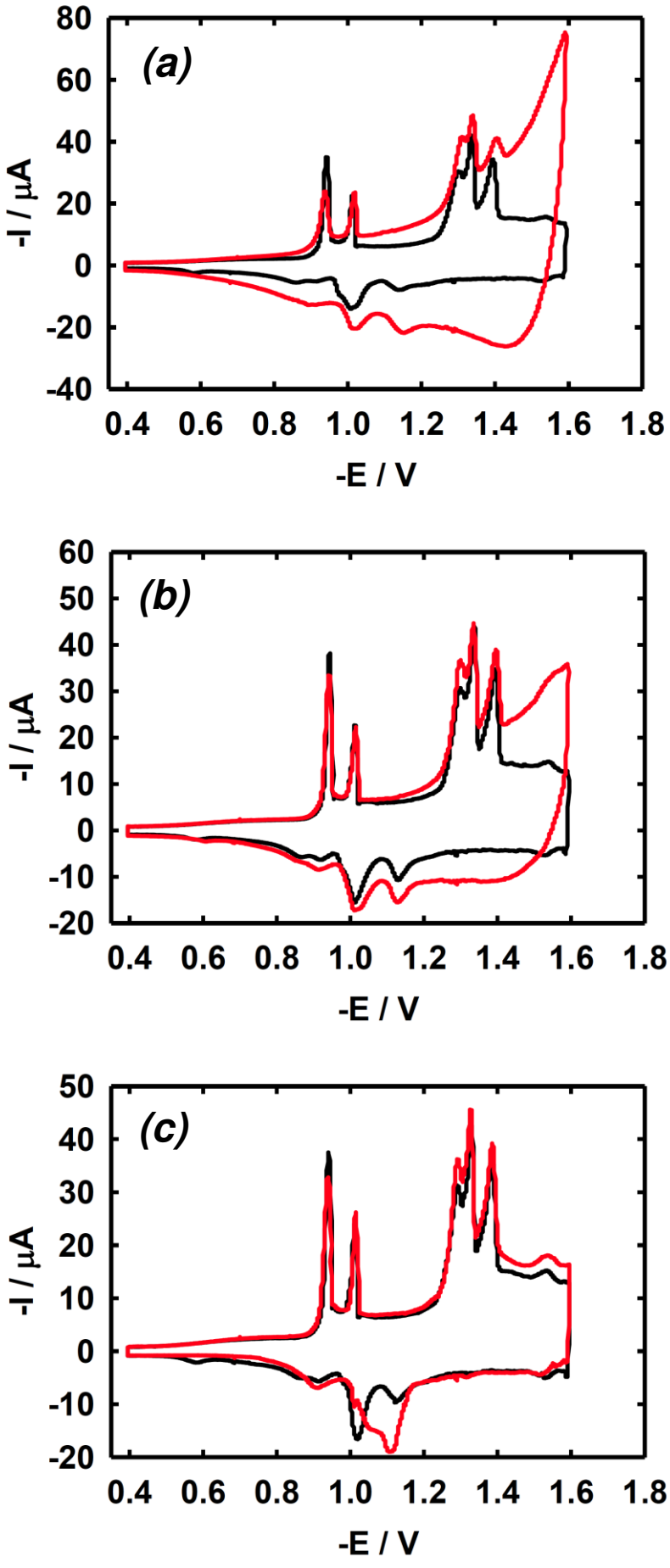
(a)
80
60
40
20
0
-20
-40
-I / µA
0.4
0.6
0.8
1.0
1.2
1.4
1.6
1.8
-E / V
(b)
60
50
40
30
20
10
0
-10
-20
-I / µA
0.4
0.6
0.8
1.0
1.2
1.4
1.6
1.8
-E / V
(c)
50
40
30
20
10
0
-10
-20
-I / µA
0.4
0.6
0.8
1.0
1.2
1.4
1.6
1.8
-E / V

5: Figure

Figure 7